Journal of Physics:
Conference Series

PURPOSE-LED
PUBLISHING™

PAPER • **OPEN ACCESS**

Site-selective ^{139}La-NQR study in bilayer nickelate $La_3Ni_2O_7$ at ambient pressure

To cite this article: Nina Seto *et al* 2026 *J. Phys.: Conf. Ser.* **3278** 012001

View the article online for updates and enhancements.

You may also like

- Microscopic Evidence of Charge- and Spin-Density Waves in $La_3Ni_2O_{7-\delta}$ Revealed by ^{139}La-NQR
Jun Luo, , Jie Feng et al.
- Doping evolution of the normal state magnetic excitations in pressurized $La_3Ni_2O_7$
Hai-Yang Zhang, Yu-Jie Bai, Fan-Jie Kong et al.
- Spin-Excitation Response to Oxygen Deficiency in $La_3Ni_2O_7$ Thin Films
Hengyang Zhong, Bo Hao, Anni Chen et al.

This content was downloaded from IP address 144.213.253.16 on 10/09/2026 at 07:37

Journal of Physics: Conference Series **3278** (2026) 012001 doi:10.1088/1742-6596/3278/1/012001

Site-selective ^{139}La-NQR study in bilayer nickelate $La_3Ni_2O_7$ at ambient pressure

Nina Seto[1], Mitsuharu Yashima[1], Masataka Kakoi[1,2], Hiroya Sakurai[3], Yoshihiko Takano[3,4], and Hidekazu Mukuda[1]

[1]Graduate School of Engineering Science, The University of Osaka, Toyonaka, Osaka 560-8531, Japan
[2]Department of Physics, The University of Osaka, Toyonaka, Osaka 560-0043, Japan
[3]National Institute for Materials Science (NIMS), Tsukuba, Ibaraki 305-0047, Japan
[4]Graduate School of Pure and Applied Sciences, University of Tsukuba, Tsukuba, Ibaraki 305-8577, Japan

E-mail: yashima.mitsuharu.es@osaka-u.ac.jp

Abstract.

To reveal the spin and charge states in the density wave order phase of bilayer nickelate $La_3Ni_2O_7$, we performed a site-selective ^{139}La-nuclear quadrupole resonance (NQR) measurement on this compound at ambient pressure. It enables us to selectively investigate the intrinsic electronic properties at the $La(2)_a$ site, which is outside the NiO_2 bilayers of the defect-free La327 crystal site. This site is clearly distinguished from the $La(2)_b$ site, which is close to some local defects. Below 150 K, nearly half of the intrinsic $La(2)_a$ sites are subject to a finite internal field parallel to the *ab* plane, while the other half are subject to a zero internal field. This is consistent with a spin density wave (SDW) ordered state of single spin-spinless stripes, which is composed by the reduced Ni magnetic moments parallel to the NiO_2-plane. We also suggest that the charge density wave order was not clearly observed at the intrinsic $La(2)_a$ site, that is, the charge distribution is nearly homogeneous around $La(2)_a$ site. This result will provide insight into the electronic states of the layered nickelates at ambient pressure, and the origin of novel superconducting states under high pressures.

1 Introduction

In 2023, High-T_c superconductivity (SC) with $T_c \sim 80$ K was discovered in the bilayer nickel oxide $La_3Ni_2O_7$ at high pressure[1]. The formal valence of Ni in $La_3Ni_2O_7$ is +2.5 ($3d^{7.5}$), indicating that the $3d_{x^2-y^2/3z^2-r^2}$ orbitals are partially occupied by three electrons per bilayer. Thus the spin, charge, and orbital degrees of freedom of the *d* electrons are expected to have some relations with the appearance of the SC state at high pressures. Previous experimental studies on $La_3Ni_2O_{7+\delta}$ (La327) have attributed anomalies in electronic states below $100 \sim 200$ K to the appearance of charge density wave (CDW) and/or spin density wave (SDW) at ambient pressure[2, 3, 4, 5, 6, 7, 8, 9, 10, 11, 12, 13, 14, 15, 16, 17, 18, 19, 20]. Among the possible density wave (DW) ordered states, the single spin-charge stripe order[9, 13, 14, 15, 18, 19](single spin-spinless stripe order [18]), the double spin-charge stripe order, the double spin stripe order[9, 16, 17], and "double charge stripe order"[20] have been proposed by various spectroscopic experiments. Nevertheless, a consensus has yet to be obtained. Additionally, the static spin order was not reported by first neutron scattering experiment[21], while a recent neutron scattering experiment by another group reported the observation of the spin orders[19].

Content from this work may be used under the terms of the Creative Commons Attribution 4.0 licence. Any further distribution of this work must maintain attribution to the author(s) and the title of the work, journal citation and DOI.
Published under licence by IOP Publishing Ltd

In the previous NMR study on La327, two crystallographically inequivalent La sites were observed in the ^{139}La-NMR spectra, as shown in Figs. 1(a) and 1(b)[11]: The La(1) is located between the NiO_2 planes and the La(2) is located outside the NiO_2 bilayers. Below T^*(∼150 K), the significant broadening of the NMR spectra and the enhancement of the nuclear spin relaxation rate ($1/T_1$) were observed, which are due to the emergence of the static *spin and/or charge* order at ambient pressure[11]. To further resolve the potential convolution of spin and charge states, a nuclear quadrupole resonance (NQR) study was demonstrated on La327 to selectively probe the local electronic states at the La(1) and La(2) sites. According to the previous NMR reports, the NQR frequency (ν_Q) was deduced to be ∼ 5.6 MHz for the La(2) and ∼2.2 MHz for La(1)[11, 17, 22]. Figure 1(c) displays the schematic of the entire ^{139}La-NQR spectrum anticipated for two different La sites above 150 K.

In this paper, we review the ^{139}La(2)-NQR study on La327($\delta \sim 0$), which revealed unambiguous evidence of SDW order with the single spin-spinless stripes below T^* (∼150 K) by selecting the intrinsic La327 crystal site microscopically[18].

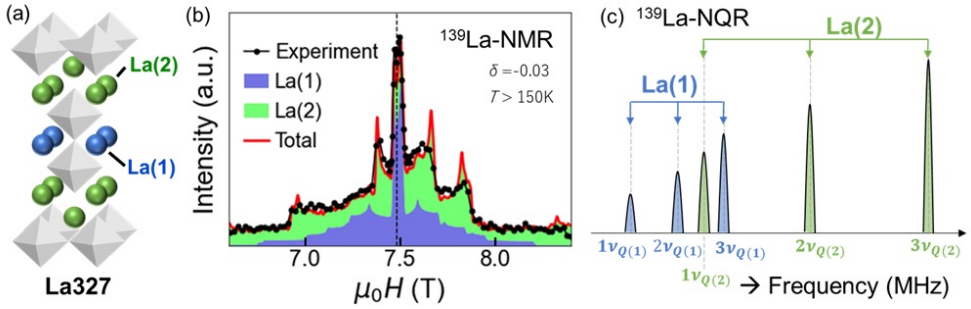


Figure 1: (Color online) (a) Crystal structure of the bilayer nickelate $La_3Ni_2O_7$ (La327). (b) Two crystallographically inequivalent La sites, La(1) and La(2), were identified by ^{139}La-NMR spectrum above 150 K[11]. This allows us to deduce the NQR frequency (ν_Q) for each La(1) and La(2) site. (c) Schematic of the expected entire ^{139}La-NQR spectrum for two different La sites, which provides an opportunity to selectively probe the La(1) and La(2) sites. This study focuses on the La(2)-NQR spectra in the frequency regions of $3\nu_Q(2)$ in Fig. 2 and from $2\nu_Q(2)$ to $3\nu_Q(2)$ in Fig. 3(a).

2 Experimental

^{139}La-NQR spectra were measured using a coarse powder sample of polycrystal La327($\delta \sim 0$) synthesized via the solid-state reaction method[24]. The oxygen deficiency, δ, is determined by thermogravimetric (TG) analysis[24]. An X-ray diffraction experiment revealed a single orthorhombic structural phase with lattice parameters reported previously[24]. For comparison, the same experiment was carried out on the oxygen-deficient polycrystal La327($\delta \sim -0.03$), which was synthesized using a different method[25]. In general, the energies of the ^{139}La nuclear spins ($I = 7/2$) are split into four levels ($m = \pm 1/2$, $\pm 3/2$, $\pm 5/2$, and $\pm 7/2$) by the nuclear quadrupole interaction, and thus, as illustrated in Fig. 1(c), three resonance peaks are expected for each La site in the NQR spectrum. Here, the NQR frequency for La(i) site is defined by $\nu_Q^{(i)} = 3eQV_{zz}^{(i)}/[2I(2I-1)h)]$, where Q is the electric quadrupole moment of ^{139}La, and $V_{zz}^{(i)}$ is a principal value of the electric field gradient (EFG) tensor at each La(i) site. The asymmetry parameter of the EFG $\eta^{(i)}$ is defined as $|V_{xx}^{(i)} - V_{yy}^{(i)}|/V_{zz}^{(i)}$. To discuss the spin and charge states from the microscopic points of view, we focus on the ^{139}La-NQR spectra at $2\nu_Q$ ($\pm 5/2 \leftrightarrow \pm 3/2$) and $3\nu_Q$ ($\pm 7/2 \leftrightarrow \pm 5/2$) of La(2) site in this study.

3 Results and discussion

In an ideal crystal of La327 without any defects, a single $3\nu_Q$-resonance peak from La(2) site is anticipated in the NQR spectrum for $T > T^*$(∼150 K). However, as shown in Fig. 2(a), two distinct peaks are observed in La327($\delta \sim 0$), which are denoted as La(2)$_a$ and La(2)$_b$. The result is compared with that of another sample of La327($\delta \sim -0.03$) in Fig. 2(b), suggesting that there are several La(2) sites due to some defects in this sample. We note that the peak of La(2)$_a$ (∼17.7 MHz at 160 K) has the narrowest linewidth and the largest intensity in both La327 samples, and thus, La(2)$_a$ is assigned to the intrinsic

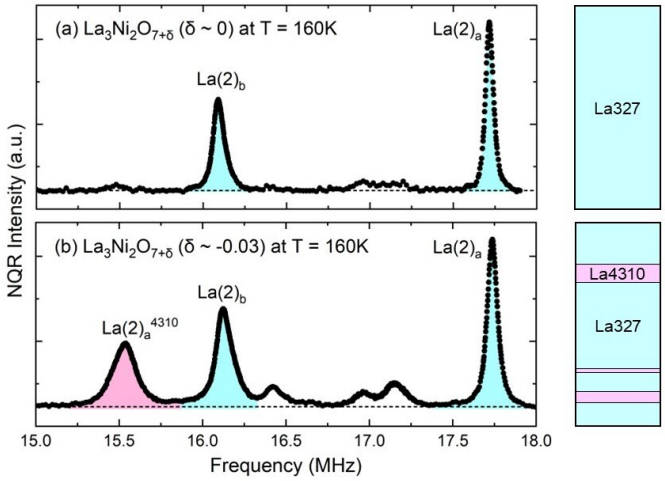


Figure 2: (Color online) La(2)-NQR spectra for $3\nu_Q$ frequency region at $T > T^*$ in (a) La327($\delta \sim 0$), compared to the results in (b) La327($\delta \sim -0.03$). If it were a perfect La327 crystal without any defects, we expect only one La(2) site that gives only one peak in this frequency region. However, in La327($\delta \sim 0$), two resonance peaks are observed: They are denoted as $\mathrm{La(2)_a}$ and $\mathrm{La(2)_b}$, which are attributed to the site of the ideal La327 and the one near some defects, respectively. The peak at $\sim$15.5 MHz is the ideal La(2) site of La4310, which are included as stacking faults as illustrated schematically in right panel. We note that the La327($\delta \sim 0$) sample includes almost no stacking faults of La4310 impurity. Cited from Ref.[18].

La(2) site in an ideal La327 crystal structure without defects around them. The peak at approximately 15.5 MHz is assigned to the $\mathrm{La(2)_a^{4310}}$ site of an ideal La4310 crystal without nearby defects[18, 22, 23]. Notably, the La327($\delta \sim 0$) sample contains almost no stacking faults of La4310 phase, although they exist in La327($\delta \sim -0.03$). Hereafter, we focus on the NQR study on the sample La327($\delta \sim 0$) ensured by good quality. In the following discussion, we focus on the results for the La327 sample ($\delta \sim 0$), which is characterized by its good quality.

Next, we present the T dependence of the $3\nu_Q$- and $2\nu_Q$-spectra to discuss the spin and charge states across T^*($\sim$150 K) at the intrinsic $\mathrm{La(2)_a}$ site of La327($\delta \sim 0$). As shown in Fig. 3(a), the $3\nu_Q$-spectrum at approximately 17.8 MHz splits slightly into two narrow peaks. On the other hand, the $2\nu_Q$-spectrum at $\sim$11.9 MHz broadens and splits into three peaks below T^*: One peak with a narrow linewidth remains around the frequency corresponding to pure NQR frequency (i,e, zero internal field), however, the other two broad peaks shift significantly to lower frequencies. This result cannot be explained primarily by the charge anomaly: When the relation $\nu_Q \propto V_{zz}$ is taken into account, the deformation of the $3\nu_Q$-spectrum should be approximately 1.5 times larger than that of the $2\nu_Q$-spectrum, if the charge anomaly such as CDW is the primary cause. Thus, we consider the case of magnetic spin order next.

To reproduce the spectra of $3\nu_Q$ and $2\nu_Q$ simultaneously, we simulated the peak-shift as a function of the internal magnetic field (H_{int}) and the angle θ between V_{zz} and H_{int}. We obtained a good result when we assumed that θ is nearly 90°. The peak frequencies calculated for $3\nu_Q$ and $2\nu_Q$ as a function of H_{int} are shown by the red curves in Fig. 3(b). The large (small) intensity expected in the spectrum is represented by the dark (light) tones on the colored curves. A small shift to lower frequency for $3\nu_Q$-peaks and a large splitting and shift for $2\nu_Q$-peaks can be simultaneously reproduced by assuming $|H_{\mathrm{int}}| \sim 0.18$ T and $\theta \sim 88.3°$[18]. In addition to the presence of the aforementioned $\mathrm{La(2)_a^{\pm}}$ sites with $H_{\mathrm{int}} \neq 0$, we must also consider the presence of $\mathrm{La(2)_a^0}$ sites with $H_{\mathrm{int}} = 0$, where H_{int} is nearly canceled out. The volume fraction of $\mathrm{La(2)_a^{\pm}}$ with $H_{\mathrm{int}} \sim \pm 0.18$ T is roughly comparable to that of $\mathrm{La(2)_a^0}$ with $H_{\mathrm{int}} = 0$.

Consequently, our NQR result is consistent with the SDW order model with single spin-spinless stripes, where the charge is nearly homogeneous. Figure 3(c) illustrates the spin structure of this model. The magnetic moments at the Ni site (M_{Ni}) are antiferromagnetically aligned in the *ab*-plane, as shown by the red and blue arrows in this figure. It induces the comparable number of $\mathrm{La(2)_a^{\pm}}$ and $\mathrm{La(2)_a^0}$ sites with $|H_{\mathrm{int}}|$ =0.18 and 0 T, which corresponds to the sites on the straight Ni-spin and spinless channels, respectively. Here, we exclude cases where M_{Ni} is parallel to the *c*-axis or not parallel to the *a*-axis within

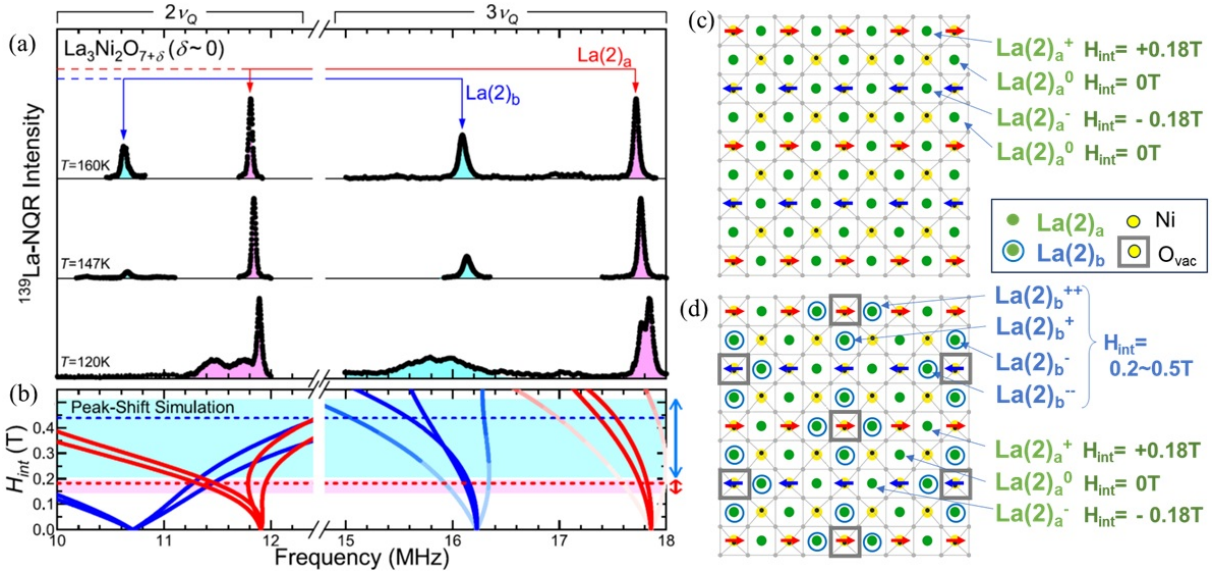


Figure 3: (Color online) (a) La(2)-NQR spectra at $2\nu_Q$ (10 ~ 12 MHz) and $3\nu_Q$ (15 ~ 18 MHz) across T^* for La327($\delta \sim 0$). (b) Simulation of resonance frequencies as a function of $H_{\rm int}$ for La(2)$_{\rm a}$(red) and La(2)$_{\rm b}$(blue). There are two La(2)$_{\rm a}$ sites with $|H_{\rm int}| = 0.18$ T and 0 T, while $H_{\rm int}$ for La(2)$_{\rm b}$ sites was distributed largely from 0.2 to 0.5 T. (c) Illustration of SDW order with a single spin-spinless stripe at the La(2)$_{\rm a}$ for the case of an ideal La327 without any defects, which consistently explains our results. The sites with $H_{\rm int} = \pm 0.18$T and 0 T are La(2)$_{\rm a}^{\pm}$ on the Ni spin channel and La(2)$_{\rm a}^{0}$ on the spinless channel, respectively. The AFM moments are aligned antiferromagnetically within the NiO_2 layers. (d) Illustration of possible spatial distribution of La(2)$_{\rm a}$ and La(2)$_{\rm b}$ around $O_{\rm vac}$s (squares) in the case of hypothetical La327 crystal with oxygen deficiencies. We deduce that the $H_{\rm int}$ at the La(2)$_{\rm b}$ sites around $O_{\rm vac}$s are inhomogeneously distributed from $H_{\rm int} \sim \pm$ 0.5 T at La(2)$_{\rm b}^{\pm\pm}$ sites on the Ni-spin channel to $H_{\rm int} \sim \pm$ 0.2 T at La(2)$_{\rm b}^{\pm}$ sites on the spinless channel. Cited from Ref.[18].

the ab plane, since the presence of the sites with $H_{\rm int}$ =0 is not explained in such situations. According to the DFT calculations, the direction of V_{zz} at La(2) is tilted approximately 20° from the c- toward the b-axis. If the magnetic moment were parallel to the b-axis, the θ would be 70°, which is not close to our experimental fact. Thus, we consider that the most likely direction of $M_{\rm Ni}$ is along the a-axis and the propagation vector $Q_{\rm SDW} = (0, 1/2)$[18].

We note that the observed value of $|H_{\rm int}| \sim$0.18 T at the La(2)$_{\rm a}$ site is one order of magnitude smaller than ~2 T observed at the La site of the antiferromagnetic order of La_2NiO_4 (La214), which possesses a high-spin state (d^8) of Ni^{2+}[26, 27]. Since the hyperfine coupling constant ($A_{\rm hf}$) is not identical to that of La214, the precise estimation of $M_{\rm Ni}$ of La327 is difficult from a simple ratio of $A_{\rm hf}$. However, the small value of $H_{\rm int}$ in La327 suggests a reduction in $M_{\rm Ni}$ due to d-electron itinerancy in metallic La327, unlike the localized system of insulating La214. According to μSR experiments, assuming $M_{\rm Ni}$ exists in the ab plane, $M_{\rm Ni} \sim 0.42\mu_{\rm B}$ was proposed[13]. Considering that our experimental result indicates that $M_{\rm Ni}$ is in the inplane direction (a-axis), we can infer a value of approximately $0.42\mu_{\rm B}$. It is similar to those recently reported in neutron scattering experiments[19] Theoretically, this SDW state can be explained by nesting of Fermi surfaces between the α and β pockets, which are formed by the hybridized bands of the bonding orbitals of the $3d_{3z^2-r^2}$ band originating from the NiO_2 bilayer and the $3d_{x^2-y^2}$ orbitals[28, 29]. The strong band hybridization effect between these two orbitals is likely related to the reduced magnetic moment.

Finally, we address the origin of the La(2)$_{\rm b}$ site, which is close to some local defects. The T dependence of the $3\nu_Q$ peak frequency and the nuclear relaxation rate $1/T_1T$ for the La(2)$_{\rm b}$ site resembles that for the La(2)$_{\rm a}$ site[18], suggesting that they belong to a similar crystallographic structure, that is, it is not attributed to the apparent phase separation. Therefore, we deduce that the La(2)$_{\rm b}$ site is most likely the site close to an oxygen vacancy ($O_{\rm vac}$) assumed to be between NiO_2 planes. Assuming one oxygen vacancy ($O_{\rm vac}$), the four adjacent La(2)$_{\rm a}$ sites (eight sites above and below NiO_2 bilayers) become La(2)$_{\rm b}$

sites, as shown in Fig. 3(d). Assuming a hypothetical crystal La327 ($\delta \sim -1/8$), the number of $La(2)_a$ and $La(2)_b$ sites would be comparable, which explains the similar spectral intensities. Below 150 K, the very broad NQR spectrum was observed at $La(2)_b$ sites, as shown in Fig. 3(a), which can be explained by the simulation assuming an inhomogeneously enhanced internal field of $|H_{int}|$ =0.2∼0.5 T in the same model[18]. This can be interpreted as $La(2)_b^{\pm\pm}$ site with strongly enhanced H_{int} on the Ni spin channel, and $La(2)_b^{\pm}$ site with moderate H_{int} on the spinless channel, as indicated in Fig. 3(d).

We note that the other NQR reports have proposed that the $La(2)_b$ may be attributed to the La(2) site in Fmmm structure (not Amam structure)[17], the La(2) site at the interface of La4310 side of the La4310/La327 stacking faults[23], and the La(2) site at the interface of La327 side of the La327/La4310 stacking faults[20]. The origin of the $La(2)_b$ site is still controversial. In our interpretation, the question also remains: Is there a specific density (e.g., δ=−1/8) that stabilizes the oxygen vacancy? and a corresponding excess oxygen somewhere such as in a Frenkel defect ? This remains a problem for the future research.

4 Summary

^{139}La(2)-NQR spectroscopy distinguishes the intrinsic $La(2)_a$ site of the ideal La327 crystal from the $La(2)_b$ site close to some local defects, which enables us to discuss the intrinsic electronic properties of La327 crystal. Through the analyses of ^{139}La(2)-NQR spectrum below 150 K, we revealed the emergence of two $La(2)_a$ sites with zero and finite internal field H_{int}. This result is consistently explained by the SDW order with single spin-spinless stripes composed of a moderately reduced antiferromagnetic moment $M_{Ni}(\parallel a)$ with $Q_{SDW} = (0, 1/2)$. We also suggest that the charge density wave order was not clearly observed, i.e. that the charge distribution is nearly homogeneous at the intrinsic La327 site. Even for the $La(2)_b$ site, the result is also explained within the same model by considering the inhomogeneous internal magnetic fields enhanced around the nearby defects. In the future, these results will provide further insight into understanding the possible relation with the high-T_c phase at high pressure in these superconducting layered nickel oxides.

Acknowledgments

This work was partially supported by the Iketani Science and Technology Foundation, Nippon Sheet Glass Foundation, Takahashi Industrial and Economic Research Foundation, and JSPS KAKENHI Grant No. JP25K00959 and JP24K01333. M.K. was supported by the Research Fellowship for Young Scientists, Grant No. JP25KJ1758. Two of the authors (H. S. and Y. T.) were supported by World Premier International Research Center Initiative (WPI), MEXT, Japan.

References

[1] H. Sun, M. Huo, X. Hu, J. Li, Z. Liu, Y. Han, L. Tang, Z. Mao, P. Yang, B. Wang, J. Cheng, D.-X. Yao, G.-M. Zhang, and M. Wang, Nature **621**, 493 (2023).

[2] Z. Zhang, M. Greenblatt, and J. B. Goodenough, J. Solid State Chem. **108**, 402 (1994).

[3] G. Q. Wu, J. J. Neumeier, and M. F. Hundley, Phys. Rev. B **63**, 245120 (2001).

[4] Z. Liu, H. Sun, M. Huo, X. Ma, Y. Ji, E. Yi, L. Li, H. Liu, J. Yu, Z. Zhang, Z. Chen, F. Liang, H. Dong, H. Guo, D. Zhong, B. Shen, S. Li, and M. Wang, Sci. China: Phys. Mech. Astron. **66**, 217411 (2023).

[5] Z. Liu, M. Huo, J. Li, Q. Li, Y. Liu, Y. Dai, X. Zhou, J. Hao, Y. Lu, M. Wang, and H.-H. Wen, Nat. Comm. **15**, 7570 (2024).

[6] J. Hou, P.-T. Yang, Z.-Y. Liu, J.-Y. Li, P.-F. Shan, L. Ma, G. Wang, N.-N. Wang, H.-Z. Guo, J.-P. Sun, Y. Uwatoko, M. Wang, G.-M. Zhang, B.-S. Wang, and J.-G. Cheng, Chin. Phys. Lett. **40**, 117302 (2023).

[7] Y. Zhang, D. Su, Y. Huang, Z. Shan, H. Sun, M. Huo, K. Ye, J. Zhang, Z. Yang, Y. Xu, Y. Su, R. Li, M. Smidman, M. Wang, L. Jiao, and H. Yuan, Nat. Phys. **20**, 1269 (2024).

[8] G. Wang, N. N. Wang , X. L. Shen, J. Hou, L. Ma, L. F. Shi, Z. A. Ren, Y. D. Gu, H. M. Ma, P. T. Yang , Z. Y. Liu, H. Z. Guo, J. P. Sun, G. M. Zhang, S. Calder , J.-Q. Yan, B. S. Wang, Y. Uwatoko, and J.-G. Cheng, Phys. Rev. X **14**, 011040 (2024).

[9] X. Chen, J. Choi, Z. Jiang, J. Mei, K. Jiang, J. Li, S. Agrestini, M. Garcia-Fernandez, X. Huang, H. Sun, D. Shen, M. Wang, J. Hu, Y. Lu, K.-J. Zhou, and D. Feng, Nat. Commun. **15**, 9597 (2024).

[10] S. Taniguchi, T. Nishikawa, Y. Yasui, Y. Kobayashi, J. Takeda, S. Shamoto and M. Sato, J. Phys. Soc. Jpn. **64**, 1644 (1995).

[11] M. Kakoi, T. Oi, Y. Ohshita, M. Yashima, K. Kuroki, T. Kato, H. Takahashi, S. Ishiwata, Y. Adachi, N. Hatada, T. Uda, and H. Mukuda, J. Phys. Soc. Jpn. **93**, 053702 (2024).

[12] Y. Meng, Y. Yang, H. Sun, S. Zhang, J. Luo, L. Chen, X. Ma, M. Wang, F. Hong, X. Wang, and X. Yu, Nat. Commun. **15**, 10408 (2024).

[13] K. Chen, X. Liu, J. Jiao, M. Zou, Y. Luo, Q.Wu, N. Zhang, Y. Guo, and L. Shu, Phys. Rev. Lett. **132**, 256503 (2024).

[14] R. Khasanov, T. J. Hicken, D. J. Gawryluk, L. P. Sorel, S. Bötzel, F. Lechermann, I. M. Eremin, H. Luetkens, and Z. Guguchia, Nat. Phys. **21**, 430 (2025).

[15] X. Ren, R. Sutarto, X. Wu, J. Zhang, H. Huang, T. Xiang, J. Hu, R. Comin, X. Zhou, and Z. Zhu, Commun. Phys. **8**, 52 (2025).

[16] N. K Gupta, R. Gong, Y. Wu, M. Kang, C. T. Parzyck, B. Z. Gregory, N. Costa, R. Sutarto, S. Sarker, A. Singer, D. G. Schlom, K. M. Shen, and D. G. Hawthorn, Nat. Commun. **16**, 6560 (2025).

[17] D. Zhao, Y. Zhou, M. Huo, Y. Wang, L. Nie, Y. Yang, J. Ying, M. Wang, T. Wu, and X. Chen, Sci. Bull. **70**, 1239 (2025).

[18] M. Yashima, N. Seto, Y. Oshita, M. Kakoi, H. Sakurai, Y. Takano, H. Mukuda, J. Phys. Soc. Jpn. **94**, 054704 (2025).

[19] I. Plokhikh, T.J. Hicken, L. Keller, V. Pomjakushin, S.H. Moody, P. Foury-Leylekian, J.J. Krieger, H. Luetkens, Z. Guguchia, R. Khasanov, D.J. Gawryluk, arXiv:2503.05287.

[20] J. Luo, J. Feng, G. Wang, N. N. Wang, J. Dou, A. F. Fang, J. Yang, J. G. Cheng, G. Q. Zheng, and R. Zhou, Chinese Phys. Lett. **42**, 067402 (2025).

[21] T. Xie, M. Huo, X. Ni, F. Shen, X. Huang, H. Sun, H. C. Walker, D. Adroja, D. Yu, B. Shen, L. He, K. Cao, and M. Wang, Sci. Bull. **69**, 3221 (2024).

[22] T. Fukamachi, K. Oda, Y. Kobayashi, T. Miyashita, and M. Sato, J. Phys. Soc. Jpn. **70**, 2757 (2001).

[23] N. N. Wang, G. Wang, X. L. Shen, J. Hou, J. Luo, X. P. Ma, H. X. Yang, L. F. Shi, J. Dou, J. Feng, J. Yang, Y. Q. Shi, Z. A. Ren, H. M. Ma, P. T. Yang, Z. Y. Liu, Y. Liu, H. Zhang, X. L. Dong, Y. X. Wang, K. Jiang, J. P. Hu, S. Nagasaki, K. Kitagawa, S. Calder, J. Q. Yan, J. P. Sun, B. S. Wang, R. Zhou, Y. Uwatoko, and J. G. Cheng, Nature **634**, 579 (2024).

[24] Y. Ueki, H. Sakurai, H. Nagata, K. Yamane, R. Matsumoto, K. Terashima, K. Hirose, H. Ohta, M. Kato, and Y. Takano, J. Phys. Soc. Jpn. **94**, 013703 (2025).

[25] Y. Adachi, N. Hatada, K. Hirota, M. Kato, and T. Uda, J. Am. Ceram. Soc. **102**, 7077 (2019).

[26] J. Rodriguez-Carvajal, M. T. Fernandez-Diaz, and J. L. Martinez, J. Phys.: Condens. Matter **3**, 3215 (1991).

[27] S. Wada, Y. Furukawa, M. Kaburagi, T. Kajitani, S. Hosoya, and Y. Yamada, J. Phys.: Condens. Matter **5**, 765 (1993).

[28] Z. Luo, X. Hu, M. Wang, W. Wu, and D.-X. Yao, Phys. Rev. Lett. **131**, 126001 (2023).

[29] Q.-G. Yang, G. M. Zhang, and F. C. Zhang, Phys. Rev. B **108**, L140505 (2023).